Particle dynamics in a virtual harmonic potential

Momčilo Gavrilov, Yonggun Jun[a], and John Bechhoefer

Department of Physics, Simon Fraser University, Burnaby, BC, Canada

August 2, 2013

ABSTRACT

Feedback traps can create arbitrary virtual potentials for exploring the dynamics of small Brownian particles. In a feedback trap, the particle position is measured periodically and, after each measurement, one applies the force that would be produced by the gradient of the "virtual potential," at the particle location. Virtual potentials differ from real ones in that the feedback loop introduces dynamical effects not present in ordinary potentials. These dynamical effects are caused by small time scales associated with the feedback, including the delay between the measurement of a particle's position and the feedback response, the feedback response that is applied for a finite update time, and the finite camera exposure from integrating motion. Here, we characterize the relevant experimental parameters and compare to theory the observed power spectra and variance for a particle in a virtual harmonic potential. We show that deviations from the dynamics expected of a continuous potential are measured by the ratio of these small time scales to the relaxation time scale of the virtual potential.

Keywords: feedback trap, ABEL trap, virtual potential, stochastic thermodynamics, Landauer's principle

1. INTRODUCTION

The recently developed feedback trap* is a device for trapping and manipulating single fluorescent particles in solution.[1] The main advantage of this device is its ability to trap molecules and other small objects directly, rather than attaching them to a micron-sized bead or encapsulating them. The feedback trap counteracts the random thermal fluctuations that perturb the motion of small objects in a finite-temperature fluid. The basic idea is to periodically measure the position of an object and then to calculate and apply a force to keep the particle in the field of view. In contrast to optical tweezers, there is no physical potential to trap the particle; rather, the action of the feedback loop creates a "virtual potential" that can confine a particle or force it to perform more complicated motion. Absent the feedback loop, there is no potential and the particle diffuses freely in a fluid cell.

Feedback traps have led to two types of study. First, they have been used to measure physical and chemical properties of single molecules. For example, one can measure the diffusion constant and electric-field mobility of single particles,[3] even ones as small as a single fluorescent dye molecule in water.[4] If the object has internal structure, one can confine its center of mass and then measure the fluctuations of diffusion coefficients,[5] along with the elastic and dissipative properties of internal modes.[6,7] More recently, the feedback trap has been used to study the chemical properties of single molecules, including photodynamic and enzymatic properties of biomolecules,[8] and to study the interplay between fluorescence spectroscopy and conformation at the single-molecule level.[9,10]

The second type of study, which has been more limited to date, is to use the feedback trap to study fundamental questions in statistical mechanics. The applications to statistical mechanics take advantage of the ability of feedback traps to impose arbitrary, time-dependent virtual potentials on particles. For example, Cohen studied the motion of a particle in a virtual double-well potential and in potentials of the form $U(r) \sim r^n$, with r the distance from a reference center.[11] The choice $n = 2$ corresponds to the familiar harmonic potential, but other

Further author information: Send correspondence to MG, momcilog@sfu.ca, or JB, johnb@sfu.ca.

[a] Present address: Department of Developmental and Cell Biology, University of California, Irvine CA 92697-2300.

* Cohen and Moerner use the name "Anti-Brownian ELectrokinetic," or ABEL trap.[1] Because the trap can counteract all types of fluctuations, not just thermal ones, and because it can do so with forces that are not necessarily electrokinetic,[2] we prefer the simpler and more general name of "feedback trap."

Optical Trapping and Optical Micromanipulation X, edited by Kishan Dholakia, Gabriel C. Spalding,
Proc. of SPIE Vol. 8810, 881012 · © 2013 SPIE · CCC code: 0277-786X/13/$18 · doi: 10.1117/12.2027238

choices are equally easy to impose. In preliminary work,[12] we have attempted to use time-dependent virtual potentials to study the Landauer Principle,[13,14] which relates information erasure to thermodynamic work.

One issue with the feedback trap is to understand carefully the motion it induces in particles. For example, it is clear that imposing a force that is the gradient of a potential $U(r)$ is not quite the same as imposing a physical potential. In a physical potential, the force adjusts continuously as the particle moves. In a virtual potential, the force is updated after a time t_s. Thus, we expect that the motion will be at best a discrete approximation to the true potential.

There have been a number of attempts to quantify the dynamics of a feedback trap. Although the complications due to a finite time t_s between updates are well understood,[15,16] there are other effects that need to be taken into account. In the present case, we focus on the consequences of finite camera exposures and the associated delays.[†] For example, estimating the diffusion constant D from measurements with camera exposures of duration t_c and measurement intervals t_s by the usual formula $\langle \Delta x^2 \rangle = 2Dt_s$ leads to a bias in the estimated diffusion coefficient.[16,19] Similarly, one needs to account for the delay t_d between the measured position and the feedback response. All of these short time scales affect the trap dynamics, in somewhat complicated ways. Until a recent effort,[20] there was no theory that completely accounted for these complications, and previous work has shown only qualitative agreement.[11,15,16]

In the present study, we test the theory of Ref. 20 experimentally, focusing on a detailed analysis of the motion of a particle in a virtual harmonic potential. We measure quantitatively not only its static properties (Boltzmann distribution), which has been previously examined, but also its dynamic properties (power spectrum), which had shown only qualitative agreement (with calculations that did not fully account for the camera exposure and delay). Beyond validating the specific calculations, the experiments show that it is possible to build a system whose behavior, at least on time scales ranging from 10 s down to 0.01 s, is well understood and successfully modeled. We were motivated to seek such a careful agreement between theory and experiment by a desire to test fundamental aspects of statistical mechanics and stochastic thermodynamics such as the Landauer principle,[13] which relates information erasure to thermodynamic work. Such experiments require precision measurements of work that are accurate to a fraction of k_BT. Since work measurements are based on the motion, a reliable theory is a prerequisite for quantitative analysis.

2. FEEDBACK TRAP DYNAMICS

We begin by defining the various parameters that play a role in the theory of particle dynamics in a virtual potential:

- *Hardware.* The first group of parameters relate to the experimental setup. They include the feedback update time t_s, camera exposure t_c, the response delay t_d, and the observational noise (standard deviation of χ per measurement). They are mostly set by hardware limitations of the equipment (camera and computer processing speeds). The observational noise depends both on the illumination source, collection optics, and intrinsic fluorophore properties of the particle.

- *Particle.* The second group of parameters relate to intrinsic properties of the particles themselves. For point-like particles lacking internal structure, these consist of the diffusion coefficient D and electric-field mobility μ.

- *Feedback.* Finally, there are parameters that relate to the shape and magnitude of the feedback loop and its imposed virtual potential. For a virtual harmonic potential, the key parameter is the feedback gain α. We will see that for small values of α, the gain is proportional to the "spring constant" of a continuous harmonic potential but that the interpretation changes for larger values of α.

[†] Some versions of the feedback trap use a single detector to time photon counts from a rapidly scanned laser beam. For such systems, there is no exposure time, although there continues to be a lag between the photon detection and the response. However, while the effectively instantaneous detection of photons and consequent lack of a finite camera exposure time simplifies some aspects of the dynamics, the Poisson statistics associated with both signal and background and the need to use sophisticated filtering techniques create difficulties of their own.[17,18]

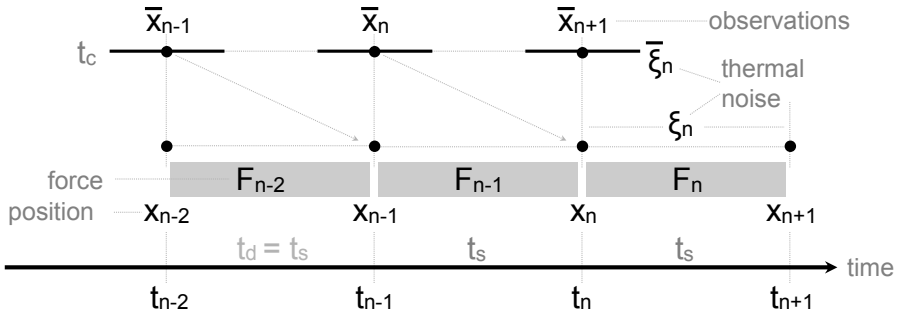

Figure 1. Timing diagram for feedback trap. The feedback update interval is t_s, and there is a delay $t_d = t_s$ between the measurement time and the output of the next feedback update. The true position of particles x_n are indicated at the bottom, together with the associated thermal noise ξ_n and force F_n. The force F_n is computed from the observed position $\bar{x}_n$ available at the time F_n is started, nt_s. At the top are indicated the observed position $\bar{x}_n$ and the amount of associated thermal noise $\bar{\xi}_n$ in each observation. For clarity, the camera exposure $t_c < t_s$, whereas in the experiments reported here, they are equal. Figure from Ref. 20.

The feedback trap uses discrete, digital feedback,[21] with time step t_s. To understand the dynamics, it is important to distinguish between the true position of the particle x_n at time n (in units of t_s) and the measured position from the camera exposure associated with time step n, which we denote $\bar{x}_n$. In particular, the feedback force at each time step, $F_n = -\alpha\bar{x}_n$, is based on the observation $\bar{x}_n$ and not on x_n.

The rather complicated timing relations amongst the true position, the measured position, and the applied force are shown in Fig. 1, for the case $t_s = t_c = t_d$, which corresponds to our experimental setup. (Choosing all three equal simplifies the formalism somewhat.) As an example of the issues that arise, we note that the force is updated from F_{n-1} to F_n midway through the camera exposure. A simple calculation[20] then shows that the measured position $\bar{x}_{n+1}$, which averages the true position over the camera exposure time, will be biased by $\frac{t_c}{8\gamma}(F_n - F_{n-1})$. It is $\bar{x}_{n+1}$ that is affected, because of the delay $t_d = t_s$.

Integrating the continuous equations of motion for $x(t)$ over t_s and applying the timing considerations of Fig. 1 then leads to coupled Langevin equations for x_n and $\bar{x}_n$:

$$\begin{aligned} x_{n+1} &= x_n - \alpha\bar{x}_n + \xi_n \\ \bar{x}_{n+1} &= x_n + \alpha'(\bar{x}_{n-1} - \bar{x}_n) + \xi_n^{(0)} + \bar{\xi}_n + \chi_n \,, \end{aligned} \tag{1}$$

where $\alpha' = \alpha\frac{t_c}{t_s}$ is a dimensionless measure of camera-exposure effects. The thermal fluctuations from the liquid bath ξ_n are integrated over the update time t_s. They are Gaussian, with $\langle\xi_n\rangle = 0$ and $\langle\xi_m\,\xi_n\rangle = 2Dt_s\,\delta_{mn}$. In a microscope, the positional noise due to the finite point-spread function of the microscope is also Gaussian, with $\langle\chi_n\rangle = 0$ and $\langle\chi_n^2\rangle = \chi^2$. ‡ There are further noise terms $\bar{\xi}_n$, which is the noise averaged over the camera exposure, and $\xi_n^{(0)}$, which accounts for the shift between the time nt_s that x_n is defined and the reference time of the corresponding camera exposure, which is taken to be the midpoint of the exposure.

Taking the Z-transform of Eq. 1 and evaluating at $z = e^{i\omega T_s}$ gives the discrete time power spectrum for particle positions in a virtual harmonic trap,

$$\left\langle|\bar{x}_n|^2\right\rangle(\omega) = \frac{2[2Dt_s + 2(\chi^2 - \frac{1}{3}Dt_c)(1-\cos\omega t_s)]}{\left|e^{2i\omega t_s} - (1-\alpha')e^{i\omega t_s} + (\alpha - 2\alpha') + \alpha' e^{-i\omega t_s}\right|^2}\,. \tag{2}$$

To find the variance $\left\langle|\bar{x}|^2\right\rangle$ of observed positions, we integrate $\left\langle|\bar{x}_n|^2\right\rangle(\omega)$ from $\omega = 0$ to $\frac{\pi}{t_s}$, the Nyquist frequency. Note that the overall factor of two in the numerator of Eq. 2 reflects our use of a one-sided power spectrum with positive frequencies only. In Ref. 20, we showed that the power spectrum in Eq. 2 and the associated variance agreed with simulations. Here, we test the agreement with a physical experiment.

‡ The camera reports quantized position and intensity measurements, but since the intensity is measured with 12-bit resolution and the point-spread function covers ≈ 16 pixels, corrections due to quantization are small and absorbed into the value of χ.

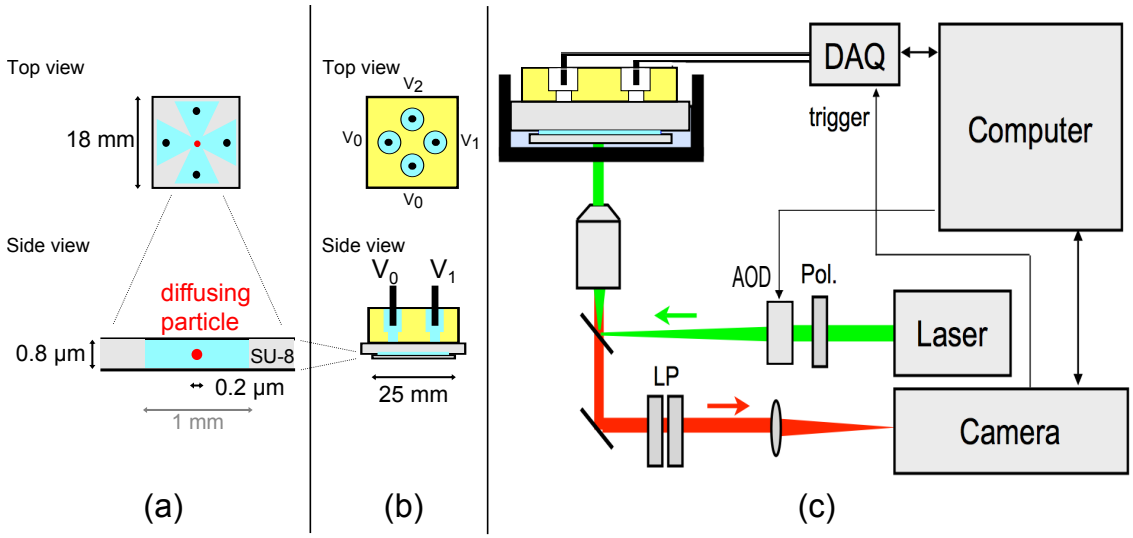

Figure 2. Schematic of experimental setup. (a) Micro-fluid cell design. The trapping area (blue) is sealed by SU-8 photoresist (gray), which also serves as an 800-nm-thick spacer. (b) Plexiglas sample holder (yellow) stores approximately 600 ml of water solution with beads in four wells (blue). One electrode (black) is placed in each well. (c) Apparatus: A camera takes images of particles in an inverted epifluorescence microscope based on a 532-nm laser. The computer sends output voltages via the DAQ to the electrodes, closing the feedback loop. POL denotes a linear polarizer, AOD an analog acousto-optic deflector, and LP denotes two long-pass filters that block residual laser reflections and transmit fluorescent light at wavelengths > 565 nm.

3. EXPERIMENTAL SETUP

Our experimental setup broadly follows that of Cohen and Moerner,[22,23] with some adaptations and simplifications. Below, we describe the overall setup and sample cell, the illumination, the image capture and processing to extract particle position, and the application of electrical forces.

The setup is designed around a home-built epifluorescence microscope made from standard optomechanical parts and incorporating a 100X, NA=1.25 oil-immersion objective (Carl Zeiss Jena, Achromat HI100x). The general setup is illustrated in Fig. 2. An 800-nm-thick flow cell was fabricated by spincoating a layer of photoresist (SU-8) on a glass surface. The SU-8 is used as a spacer rather than as simply a mask for etching. To bond the SU-8, we heat the sample to 180 °C and firmly press the cover glass onto the SU8-coated base plate.[24] The base plate was first drilled with 1 mm glass holes for the electrodes. Compared to the cells used by Cohen and Moerner,[22,23] the present design is simpler, as there is no etching of the glass. One small difference is that in our design, the triangle-shaped areas in Fig. 2 are 800 nm thick (and not 20 μm, as in Ref. 22); as a result, there is a greater voltage drop before reaching the central experimental chamber (the square 1×1 mm region in Fig. 2). However, in our experiments, we were not limited by field strengths.

We use a 5-mW, 532-nm laser (Z-Bolt, DPSS-5M) for illuminating particles. Under laser illumination, particles photobleach. To maximize the observation time, we minimize the illumination area so that particles outside the field of view are not illuminated unnecessarily. We set the illumination area by using an analog acousto-optic deflector, or AOD (AA Opto-Electronic, Model DTSXY-250-532), to rapidly scan a tightly focused laser beam at a rate of 100 kHz (x-axis) and 61.8 kHz (y-axis). The frequency ratio is chosen to be near the golden ratio, $\frac{1}{2}(1-\sqrt{5}) \approx 0.618$, which is the number that is "closest" to an irrational number in the sense that any finite approximation will have a high rational denominator. The resulting Lissajous figure for the beam thus covers relatively evenly the entire field of view.[25] The AOD has the important side benefit that moving the beam rapidly averages out speckle, improving the homogeneity of the illumination. We image fluorescent polystyrene divinylbenzene particles that are 200 nm in diameter (Thermo Scientific, R200 Fluoro-Max Fluorescent Particles, dyed red) in deionized water.

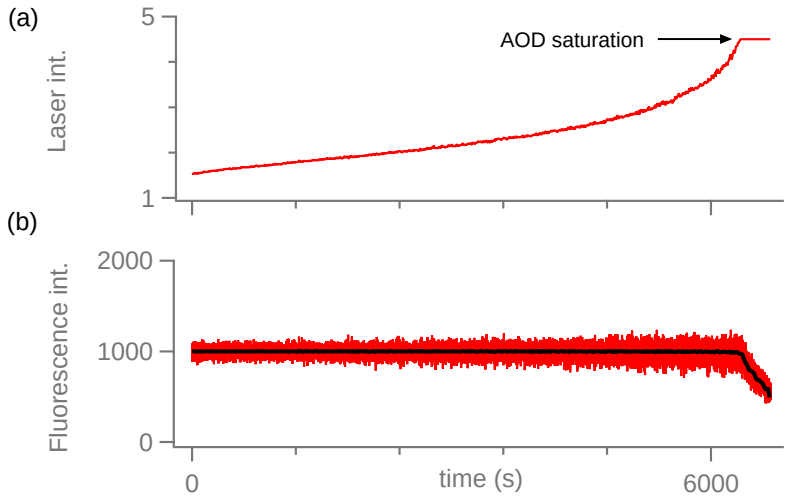

Figure 3. Proportional-integral control of the fluorescence light intensity. The decrease in fluorescence intensity due to photobleaching was compensated by increasing illumination laser intensity. a) Illumination laser intensity increases with time up to the saturation point. b) The intensity of fluorescence light (red lines) is kept constant by the AOD. Black solid line represents the intensity averaged over 20 seconds. After the AOD saturates, the intensity decreases. All intensity values are given in arbitrary units.

A further significant advantage of the AOD is that we can alter the intensity to compensate for the photobleaching of the fluorescent particle.[26] Since the observational noise χ depends on the particle's fluorescent intensity, regulating that intensity meant that the noise statistics did not drift with time. To stabilize the observed fluorescent intensity, we first time averaged the particle intensity signal using a running-average filter with time constant 2 s. The intensity fluctuations mostly result from the vertical motion of the 200 nm particle in the 800 nm trap. As the particle diffuses up and down vertically, it samples a laser beam whose intensity varies. We fed the time-averaged particle position into a proportional-integral control algorithm that adjusted the AOD intensity, which in turn regulated the intensity of the deflected laser beam. Figure 3 shows time traces of the laser illumination intensity and the observed fluorescence. The typical lifetime is about two hours, which was long enough that we could measure the effect of feedback gain variations on a single particle.

We use an electron-multiplying CCD (EMCCD) camera (Andor iXon DV-885) to acquire 100 $\times$ 100 pixel (8 $\times$ 8 μm) images at 100 Hz, with an exposure time $t_c = 10$ ms and 2 $\times$ 2 pixel binning. We recall that the control program must not only acquire images but must also, for each image acquired, find the position of the particle, compute a response, and output the appropriate voltages to the electrodes.

The camera exposure (and overall experiment) is controlled via a program written in LabVIEW (2009), with the image analysis routines written in Mathscript (a Matlab-compatible language). To estimate the particle position, we use a simplified version of the centroid algorithm of Berglund et al.[27] In our version, we first estimate the position of the particle by locating the pixel of maximum intensity. We then center a region-of-interest box around the first estimate and use the centroid algorithm to make a more precise estimate. Using an approximately centered region of interest reduces to negligible values the bias discussed in Ref. 27.

After estimating the position, the algorithm calculates the displacement of the particle from its desired position and applies the electric field needed to bring the particle to the desired position during the interval t_s. The force is created by applying voltages across two pairs of Pt80/Ir20 electrodes (0.25 mm in diameter, Goodfellow Corp.), as depicted in Fig. 2. The delay time between estimating the position and applying the force is set to $t_d = 10$ ms.

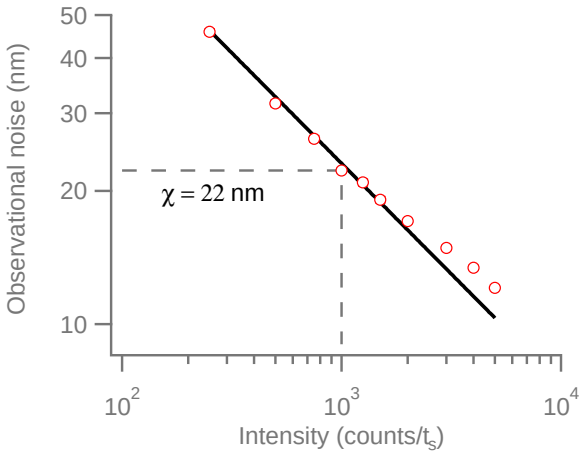

Figure 4. Observational noise χ as a function of fluorescent light intensity. The red markers are measurements on immobilized beads. The black solid line is a fit to the $\chi \sim I^{-0.5}$ power law expected for shot-noise-limited images. The dashed line indicates typical operating conditions.

4. APPARATUS AND PARTICLE PROPERTIES

We need to characterize the various parameters that affect the observed particle dynamics. As discussed in Sec. 2, the relevant parameters are grouped into hardware, particle, and feedback classes. We begin with the hardware parameters (observational noise and timing) and then proceed to the particle parameters (mobility and diffusion). The feedback parameters are known exactly, since they are set by the program.

4.1 Apparatus parameters

The observational noise χ depends on the microscope point spread function, camera pixel size, camera read and background noise, image background variations, and the intensity of the fluorescent light emitted by particle. We characterized its magnitude by immobilizing a 200-nm fluorescent bead on a glass surface and repeatedly measuring its position. Regulating the incident laser intensity I_L as shown in Fig. 3, we measured the standard deviation as a function of the observed mean fluorescence intensity. The result, Fig. 4, approximately follows the expected $I^{-0.5}$ power law expected for shot noise, with excess noise at higher intensities. We typically regulated the fluorescence intensity to a level of 1000, which corresponds to $\chi \approx 22$ nm and a particle "lifetime" of about two hours. These values are a compromise, in that maximizing I_L reduces observational noise, while minimizing I_L increases particle lifetime. Finally, drifts in the focus alter χ slowly, as may be noticed in Fig. 3(b).

The timing parameters were determined by temporarily adding an LED light between the LP filter and the camera (Fig. 2). Using the digital output from a data acquisition card (DAQ), we generated a $\tau = 0.1$ ms LED light pulse each 60 ms, as verified using a photodiode. The DAQ's analog output was set to be proportional to the light intensity detected by the camera. The analog output, camera trigger, and τ pulse were all measured by an independent DAQ and computer, sampling at 1 kHz. By adjusting the phase of the τ pulse relative to the camera trigger, we could make the pulse straddle the end of one exposure and the beginning of the next. Since this was possible with a 0.1 ms light pulse, we conclude that the "dark time" between end of one exposure and the beginning of the next was less than this time, which is short compared to the 10 ms exposure time. Thus, we conclude that $t_c = t_s = 10$ ms. The response delay t_d is evaluated by measuring the time difference between the τ pulse straddling two exposures and the time that the DAQ voltage is updated. We set the DAQ update so that $t_d = t_s$. One potential ambiguity is that a delay of an integer multiple of t_s could appear (as in aliasing) to be a shorter, fractional delay. We resolved this potential ambiguity by sending a pulse every 60 ms, or 6 time steps.

4.2 Particle parameters

The mobility measures the particle response to the electric field created by the four electrodes. In the simple 1D case with two electrodes, the applied voltage V leads to an electric force F that, in time t_s, will displace the

particle of charge q by an amount Δx, which goes from the observed position $\bar{x}$ to desired position x_0. With linear response and overdamped dynamics, $F = \gamma v$, with γ the fluid drag coefficient and $v = \Delta x/t_s$ the velocity. Introducing the electric-field mobility $\mu = \frac{q}{\gamma}$, we have $\Delta x = \mu t_s c V$, where the constant c relates the electric field to the voltage. That is, $E \equiv cV$. Since we do not try to calculate the field, we simply absorb all constants in a single parameter Λ and write $\Delta x = \Lambda V$.

In two dimensions, there are two voltages V_1 and V_2 that are applied approximately along the x- and y-coordinate axes, which are defined by the camera pixels. However, because of the complex sample geometry, the fields created by each pair of electrodes will neither be equal in magnitude nor orthogonal in direction. Thus,

$$\begin{pmatrix} \Delta x \\ \Delta y \end{pmatrix} = \Lambda \begin{pmatrix} M_{x1} & M_{x2} \\ M_{y1} & M_{y2} \end{pmatrix} \begin{pmatrix} V_1 \\ V_2 \end{pmatrix} \tag{3}$$

where Λ again is proportional to the mobility and to t_s. The matrix $\mathbf{M}$ contains information relating to the electric field vectors at the point of observation and is defined so that $\det \mathbf{M} = 1$. If we observe different particles at the same position, they will all share the same value of $\mathbf{M}$ but will have different values of Λ, reflecting the unique size and charge of each particle. Indeed, measuring 20 different particles showed a variation of 6.5%, as shown in Fig. 5(a).

We measured the one-dimensional particle diffusion coefficient by observing the variance $\langle \Delta \bar{x}^2 \rangle$ of particle displacements $\Delta \bar{x}_k = \bar{x}_k - \bar{x}_{k-1}$ and then calculating $D = \frac{\langle \Delta \bar{x}^2 \rangle - 2\chi^2}{2t_s(1 - t_c/3t_s)}$, which corrects for the camera exposure time and observational noise.[16,19] The factor of two in front of the observational noise variance arises because a displacement is calculated from two images. Figure 5(b) shows that sampling different, nominally identical particles leads to a relative variation in D of $\approx 3\%$, which corresponds to the same relative variation in radius r.

In a liquid of infinite extent, the diffusion coefficient D for spherical particles of radius r in a liquid of viscosity η is given by the Stokes-Einstein[28] formula, $D = \frac{k_B T}{6\pi\eta r}$. Near walls, the extra drag due to enhanced shear reduces the diffusion coefficient by up to a factor of two, depending strongly on the thickness of the particular sample cell.[29–31] The diffusion coefficient also depends on temperature, both explicitly in the numerator and, implicitly, through the temperature dependence of the viscosity $\eta(T)$. The viscosity effect dominates and leads to a variation in D (far from a wall) that ranges from 2.2 to 2.6 $\mu\text{m}^2/\text{s}$ for $23 < T < 26$ °C.

5. EXPERIMENTAL RESULTS

Having devised a way to calibrate the various quantities that enter into the dynamics, we are now ready to examine carefully the particle's motion in virtual potentials. We focus on a quadratic (harmonic) potential. In Sec. 5.1, we study the variance of motion in a harmonic virtual potential. In Sec. 5.2, we study the power spectrum in the same potential. Finally, in Sec. 5.3, we examine briefly motion in a double-well potential.

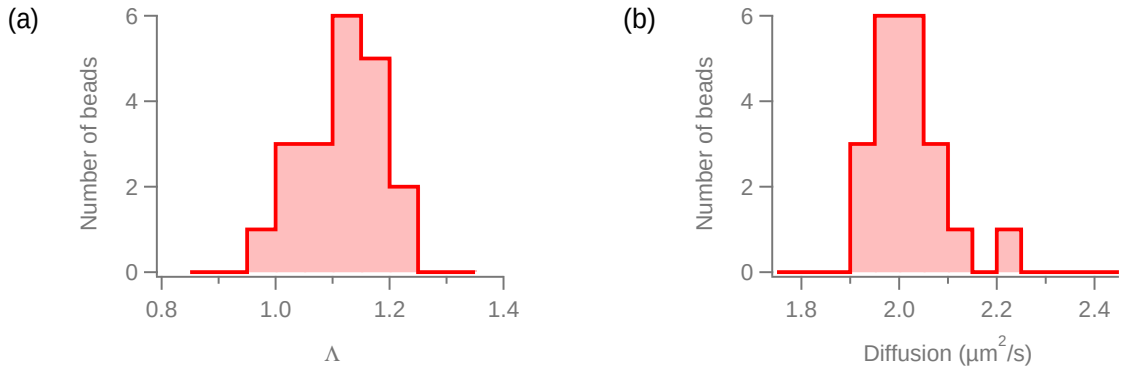

Figure 5. Variation among 20 nominally identical particles. (a) Variation in mobility scaling factor: $\langle \Lambda \rangle = 1.10 \ \frac{\mu m}{Vs}$ and $\sigma_\Lambda = 0.071 \ \frac{\mu m}{Vs}$, implying $\sigma_\Lambda / \langle \Lambda \rangle \approx 6.5\%$. (b) Variation in diffusion coefficient: $\langle D \rangle = 1.97 \ \frac{\mu m^2}{s}$, with standard deviation $\sigma_D = 0.058 \ \frac{\mu m^2}{s}$, implying $\sigma_D / \langle D \rangle \approx 2.9\%$.

5.1 Virtual harmonic potential: statics

We have observed particle dynamics in a harmonic trap for several different values of feedback gain α, as shown in Fig. 6. For $\alpha \lesssim 0.1$, the data closely approximate $1/\alpha$, which is equivalent to the equipartition relation $\langle x^2 \rangle = k_B T/k$ for spring constant k. For higher values of α, the variance begins to increase, before diverging at the (predicted) value $\alpha \approx 1.14$. The instability results from the overcorrection of perturbations.[20] In our measurements, we were limited from exploring $\alpha < 0.05$ by the small field of view in our trapping algorithm and from exploring $\alpha > 0.9$ by the too-frequent Kramers escape of the particle near the instability.

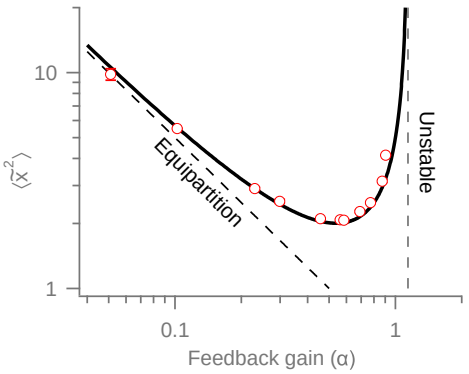

Figure 6. Experimental data showing the dimensionless position variance $\langle \tilde{x}^2 \rangle \equiv \left(\langle \tilde{x}^2 \rangle - 2\chi^2 \right)/2Dt_s$ as a function of feedback gain, based on ten minutes' data per point. Measurements on several different particles. The black solid line is generated by integrating Eq. 2 up to the Nyquist frequency, with $\chi = 0$. The equipartition relation is given by the dashed line. The vertical dashed line depicts the instability expected for $\alpha \gtrsim 1.14$.

5.2 Virtual harmonic potential: dynamics

In Fig. 7, we show the results of measurements of power spectra for low ($\alpha = 0.1$) and high ($\alpha = 0.9$) feedback gains. The solid curves are fits with only the particle parameters (D and μ) free. (We calibrated the system parameters using particles whose parameters were slightly different, so that only the intrinsic particle parameters need be determined for each measurement.) We note that the form of the spectrum agrees very well with the predicted shape. Attempting fits that use the alternate forms of the power spectrum previously proposed leads to systematic deviations.

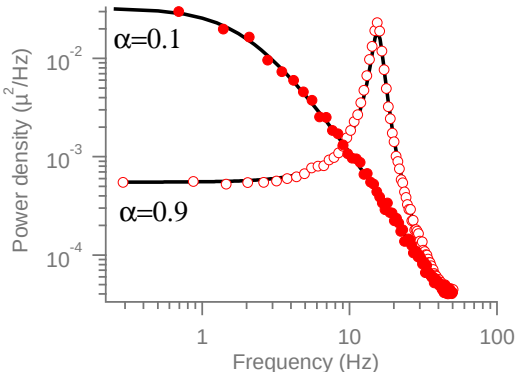

Figure 7. Power spectra for two different stiffnesses of a virtual harmonic potential. Solid markers correspond to the case of low feedback gain ($\alpha = 0.1$). Hollow markers correspond to high feedback gain ($\alpha = 0.9$). Measurements were done on two different particles with diffusion constant $D \approx 1\ \mu\text{m}^2/\text{s}$. The update time, exposure time, and delay were all set to 0.01 s. Observational noise was $\chi = 25$ nm for an intensity of $I = 1000$ counts/t_s.

5.3 Arbitrary potentials

One of the main points of interest of a feedback trap is its ability to impose arbitrary time-dependent potentials on particle. Here, we explore briefly a static double-well potential, which we parametrize as

$$\frac{U(x)}{k_BT} = 4\left(\frac{E_b}{k_BT}\right)\left[-\frac{1}{2}\left(\frac{x}{x_m}\right)^2 + \frac{1}{4}\left(\frac{x}{x_m}\right)^4\right]. \tag{4}$$

In Eq. 4, energies are scaled by k_BT and lengths by x_m, the distance between the barrier maximum and the well minimum. Figure 8(a) shows an example of the particle dynamics in such a static double-well potential. In Fig. 8(b), we show the potential $U(x)$ measured as the Boltzmann distribution $p(x) \propto e^{-\frac{U(x)}{k_BT}}$. The solid line is a fit to Eq. 4, given parameters that differ from the imposed values by $< 2\%$.

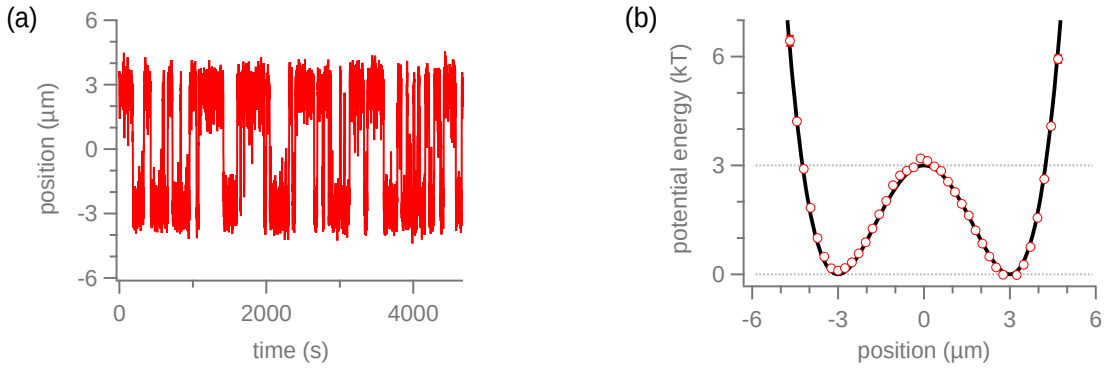

Figure 8. Motion of a particle in a virtual double-well potential. (a) Time series showing 30 spontaneous barrier hops in 83 min. The distance from the barrier center to each well was $x_m = 3$ μm. (b) Potential energy of a particle in DW potential. The potential was reconstructed using Boltzmann distribution of position measurement. The imposed energy barrier height was $E_b/k_BT = 3$, and the wells were set at $x_m = 3$ μm. A least-squares fit gives $E_b/k_BT = 3.061 \pm 0.002$ and $x_m = 3.005 \pm 0.001$ μm.

6. CONCLUSION

In this paper, we have reviewed the detailed theory of the dynamics of particles in feedback traps, concentrating on the case of a virtual harmonic potential. We have outlined the numerous steps required to reach quantitative agreement. At the present stage of our experiments, we have shown quantitative agreement between the predicted and observed power spectra, on time scales ranging between 0.01 s and 1 s. This represents the first time, to our knowledge, that a complete theory of the dynamics has been given. Previous work has always shown systematic distortions in the shape of the measured power spectra relative to predictions. We can ascribe at least part of the discrepancy now to the failure to account correctly for the effects of camera exposure and timing delays in the feedback loop. Perhaps the most important point to make, though, is that all of these complications are small and not too important, as long as we respect the condition that all three time scales must be short compared to the relaxation time in the potential. As long as those conditions are satisfied, we can view the dynamics as being very close to the continuous potential that is being imitated.

At slower time scales, we begin to notice drifts, which we tentatively ascribe to electrochemical modifications of the electrodes and, secondarily, to thermal drifts of the apparatus itself. For time scales of a few minutes or less, these effects are small. However, in attempts to measure the thermodynamic cost of information erasure ($k_BT \ln 2$/bit, measured over times of up to 10 min. per cycle and averaged over many cycles), we see significant systematic errors. These will need to be reduced in order to explore carefully the interrelationships between feedback, information, and thermodynamics.

Another topic in the analysis of motion in a feedback trap that deserves more attention is the status of thermodynamic measurements. In Ref. 20, we showed in a particular case that the work that a time-dependent

potential exerts on a particle is accurate to $\mathcal{O}(\alpha)$. That is, there are corrections to the measured work that are proportional to the ratio of the small time scale t_s to the relaxation time in the potential. These corrections mirror those that we found in comparing the exact power spectrum to that calculated for a continuous potential. By contrast, the calculations for heat that the particle dissipates into the surrounding bath reveal that the $\mathcal{O}(\alpha)$ corrections are also proportional to the total measurement time. The apparent dissipation can then become large if the motion is measured for a long time. In recent work, Sivak et al.[32] have shown that generically such effects arise because the finite time update algorithm does not properly conserve energy in the Hamiltonian part of the dynamics. This issue affects the calculation of the heat but not that of the work. It is an interesting question whether modifications to the feedback algorithm analogous to the modified numerical integrators discussed by Sivak et al.[32] can eliminate such secular terms. In any case, a full experimental test of the accuracy of thermodynamic measurements awaits future investigation.

ACKNOWLEDGMENTS

We thank Byron Gates for helpful discussions. The microfluidic flow cell was fabricated in the 4D LABS facilities at Simon Fraser University. This work was supported by NSERC, Canada.

REFERENCES

[1] Cohen, A. E. and Moerner, W. E., "Method for trapping and manipulating nanoscale objects in solution," *App. Phys. Lett.* **86**, 093109 (2005).

[2] Armani, M. D., Chaudhary, S. V., Probst, R., and Shapiro, B., "Using feedback control of microflows to independently steer multiple particles," *J. Microelectromech Syst.* **15**, 945–956 (2006).

[3] Cohen, A. E. and Moerner, W. E., "Suppressing Brownian motion of individual biomolecules in solution," *PNAS* **103**, 4362–4365 (2006).

[4] Fields, A. P. and Cohen, A. E., "Electrokinetic trapping at the one nanometer limit," *PNAS* **108**, 8937–8942 (2011).

[5] Cohen, A. E. and Moerner, W. E., "Internal mechanical response of a polymer in solution," *Phys. Rev. Lett.* **98**, 116001 (2007).

[6] Cohen, A. E. and Moerner, W. E., "Principal-components analysis of shape fluctuations of single DNA molecules," *PNAS* **104**, 12622–12627 (2007).

[7] Goldsmith, R. H. and Moerner, W. E., "Watching conformational- and photodynamics of single fluorescent proteins in solution," *Nature Chemistry* **2**, 179–186 (2010).

[8] Wang, Q., Goldsmith, R. H., Jiang, Y., Bockenhauer, S. D., and Moerner, W., "Probing single biomolecules in solution using the anti-Brownian electrokinetic (ABEL) trap," *Acc. Chem. Res.* **45**, 1955–1964 (2012).

[9] Wang, Q. and Moerner, W. E., "Lifetime and spectrally resolved characterization of the photodynamics of single fluorophores in solution using the anti-Brownian electrokinetic trap," *J. Phys. Chem. B* **117**, 4641–4648 (2013).

[10] Schlau-Cohen, G. S., Wang, Q., Southall, J., Cogdell, R. J., and Moerner, W. E., "Single-molecule spectroscopy reveals photosynthetic LH2 complexes switch between emissive states," *PNAS* **110**, 10899–10903 (2013).

[11] Cohen, A. E., "Control of nanoparticles with arbitrary two-dimensional force fields," *Phys. Rev. Lett.* **94**, 118102 (2005).

[12] Cho, A., "One cool way to erase information," *Science* **332**, 171 (2011).

[13] Landauer, R., "Irreversibility and heat generation in the computing process," *IBM Journal of Research and Development* **5**, 183–191 (1961).

[14] Bérut, A., Arakelyan, A., Petrosyan, A., Ciliberto, S., Dillenschneider, R., and Lutz, E., "Experimental verification of Landauer's principle linking information and thermodynamics," *Nature* **483**, 187–190 (2012).

[15] Gosse, C. and Croquette, V., "Magnetic tweezers: Micromanipulation and force measurement at the molecular level," *Biophys. J.* **82**, 3314 – 3329 (2002).

[16] Cohen, A. E., *Trapping and Manipulating Single Molecules in Solution*, PhD thesis, Stanford University (2006).

[17] Wang, Q. and Moerner, W. E., "Optimal strategy for trapping single fluorescent molecules in solution using the ABEL trap," *Appl. Phys. B* **99**, 23–30 (2010).

[18] Fields, A. P. and Cohen, A. E., "Optimal tracking of a Brownian particle," *Opt. Express* **20**, 22585–22601 (2012).

[19] Savin, T. and Doyle, P. S., "Static and dynamic errors in particle tracking microrheology.," *Biophys. J.* **88**, 623–638 (Jan. 2005).

[20] Jun, Y. and Bechhoefer, J., "Virtual potentials for feedback traps," *Phys. Rev. E* **86**, 061106 (2012).

[21] Bechhoefer, J., "Feedback for physicists: A tutorial essay on control," *Rev. Mod. Phys.* **77**, 783–836 (2005).

[22] Cohen, A. E. and Moerner, W. E., "The anti-Brownian electrophoretic trap (ABEL trap): Fabrication and software," *Proc. SPIE* **5699**, 296–305 (2005).

[23] Cohen, A. E. and Moerner, W. E., "An all-glass microfluidic cell for the ABEL trap: Fabrication and modeling," *Proc. SPIE* **5930**, 191–198 (2005).

[24] Serra, S. G., Schneider, A., Malecki, K., Huq, S. E., and Brenner, W., "A simple bonding process of SU-8 to glass to seal a microfluidic device," *4M 2007 - Third international Conference on multi-material micro manufacture - Proceedings* , 43 – 46 (2007).

[25] Hardy, G. H. and Wright, E. M., [*An Introduction to the Theory of Numbers*], Oxford Univ. Press, 6th ed. (2008).

[26] McHale, K. and Mabuchi, H., "Precise characterization of the conformation fluctuations of freely diffusing DNA: Beyond Rouse and Zimm," *J. Am. Chem. Soc.* **131**, 17901–17907 (2009). PMID: 19911791.

[27] Berglund, A. J., McMahon, M. D., McClelland, J. J., and Liddle, J. A., "Fast, bias-free algorithm for tracking single particles with variable size and shape," *Opt. Express* **16**, 14064–14075 (2008).

[28] Russel, W. B., Saville, D. A., Schowalter, and Raymond, W., [*Colloidal dispersions*], Cambridge University Press (1989).

[29] Faucheux, L. P. and Libchaber, A. J., "Confined Brownian motion," *Phys. Rev. E* **49**, 5158–5163 (1994).

[30] Lin, B., Yu, J., and Rice, S. A., "Direct measurements of constrained Brownian motion of an isolated sphere between two walls," *Phys. Rev. E* **62**, 3909–3919 (2000).

[31] Benesch, T., Yiacoumi, S., and Tsouris, C., "Brownian motion in confinement," *Phy. Rev. E* **68**, 021401+ (2003).

[32] Sivak, D. A., Chodera, J. D., and Crooks, G. E., "Using nonequilibrium fluctuation theorems to understand and correct errors in equilibrium and nonequilibrium simulations of discrete Langevin dynamics," *Phys. Rev. X* **3**, 011007 (2013).